

## Calibration Uncertainty Evaluation of D-Dot Sensors

Fanghong Huang\*, Youjie Yan, Jin Chen, Zhen Liu, and Binwen Wang

**Abstract**—D-dot sensor is a type of differential sensor that is widely used in the measurement of ultra-wide band (UWB) pulse electric field. The output of the sensor needs to be integrated to rebuild the original electric field. According to the methods of integration, the measurement system based on D-dot sensor can be classified into software integral D-dot measurement (SIDM) system and hardware integral D-dot measurement (HIDM) system. For an SIDM system, the accuracy of calibration, which is influenced by the integral error of the recovery signal, unfortunately, remains an impediment to its practical application. In this paper, a calibration uncertainty evaluation method based on a standard field generating equipment of time-domain electromagnetic pulse is investigated. The level of the integral error is determined by constructing a noise model using the calibration method. In the process of modeling, the characteristics of the background noise are analyzed first. Additionally, a random signal model taking background noise into account is built, and the integral value of the background noise is derived. Moreover, the integral error model is verified by a statistical method using tested data. After modeling, the uncertainty of the equivalent area for a real D-dot sensor in a software integral system and the methods for reducing the uncertainty are illustrated according to the integral error model.

### 1. INTRODUCTION

Ultra-wide band electromagnetic pulse field is a kind of transient electromagnetic field, and the rise time of the field is from dozens to hundreds of picoseconds or even shorter. Owing to a steep rise in edge, wide spectrum, and strong penetrability, the pulse is widely used in electronic jamming, target detection, and object recognition [1–3]. Measurement is one of the most important techniques for ultra-wideband electromagnetic pulse. So far, sensors used in measuring the ultra-wide band electromagnetic pulse include: TEM horn [1, 2], electro-optical sensor [4, 5], monopole, D-dot sensor [6–10], etc.

D-dot sensor has a wide spectrum and small dispersion, making it suitable for the measurement of ultra-wide band electromagnetic pulse. The sensor is suitable for measuring narrow spaces because it has a small volume. It is also suitable as a transfer standard for ultra-wide band electromagnetic field because of its stability and fidelity. A D-dot measurement system consists of D-dot sensor, signal transmission system, sampling system, data process system, etc. Most importantly, the evaluation of equivalent area and the uncertainty of equivalent area are crucial for a high accuracy measurement.

The output of the sensor is the differential signal of electric field [6, 7]; therefore, the origin pulse electric field is recovered by the integral of the output. Universal integral methods include hardware and software integrals [7]. When the ultra-wide band pulse signal of the ns-scale pulse width is measured by the hardware integral method, the amplitude of the output is quite small because of the very short integral time. Although bigger size poles are necessary in obtaining higher output amplitude, the frequency band will decrease as the size increases. Therefore, the application of hardware integral is limited.

---

*Received 5 October 2018, Accepted 14 December 2018, Scheduled 15 April 2019*

\* Corresponding author: Fanghong Huang (570059217@qq.com).

The authors are with the Northwest Institute of Nuclear Technology, Xi'an 710024, China.

When the software integral method is applied, the noise in the direct output signal will be accumulated at the integral error. The integral error of the D-dot measurement system has been studied by various researchers. Yao [10] et al. proposed a linear-fitting compensation method to reduce the integral error in D-dot system. The bias of the direct output signal was eliminated by the method, but the uncertainty of this method has not been evaluated.

The uncertainty of the equivalent area of the D-dot sensor in a software integral measurement system is evaluated in this paper. The main focus of this paper is to elucidate on the uncertainty of the integral pulse signal using the software integral method.

## 2. MODEL OF UNCERTAINTY EVALUATION FOR THE CALIBRATION OF THE D-DOT SENSORS

The D-dot sensor evaluated in this paper was developed in our own institution (Figure 1). The calibration equipment is a standard field generating equipment of time-domain electromagnetic pulse [11, 12, 17], which consists of a mono-cone field forming system, bipolar-pulse voltage source, high-speed digital oscilloscope, coaxial lines, and positioning fixture (Figure 2). Therefore, the D-dot sensor in a software integral system is calibrated by the standard electric field generated by the equipment.

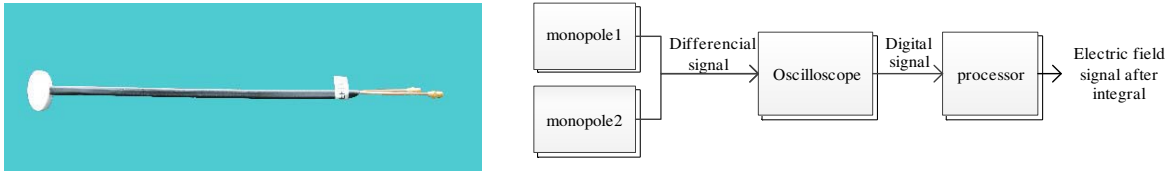


**Figure 1.** Schematic illustration of the D-dot sensor and the structure of the measurement system.

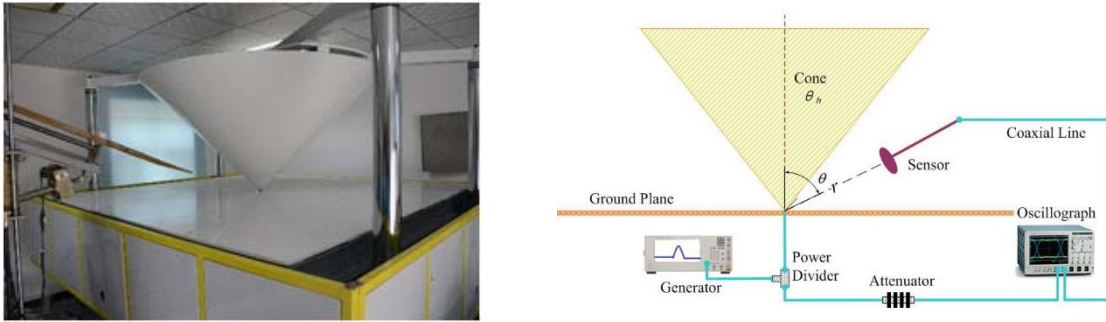


**Figure 2.** Physical figure and structure of the calibration system.

The equivalent area  $A_{eq}$  of a D-dot sensor can be achieved by the equation as follows,

$$A_{eq} = \frac{\int V_o(t)dt}{\varepsilon Z_L E(t)} = \frac{\left( \sum_{k=1}^n V_o(k) \right)_{p-p}}{\varepsilon Z_L (E(k))_{p-p}} = \frac{V_{I,p}}{\varepsilon Z_L E_p} \quad (1)$$

where  $V_o(t)$  is the direct output signal of the D-dot system;  $E(t)$  is the electric field signal;  $V_o(k)$  is the discrete signal of  $V_o(t)$  obtained by digital oscilloscope;  $E(k)$  is the discrete signal of  $E(t)$ . The calculation method of  $E(t)$  is introduced from [11, 12], so it is not described in detail in this paper, and the division operation between  $\int V_o(t)dt$  and  $E(t)$  means calculating a ratio between the two signals (on condition that they have the same waveform).  $p-p$  is the peak-peak value of the bipolar pulse, and the ratio calculation between the peak-peak values of the two signals is a simplified method for calculating the ratio between the two signals.  $Z_L$  is the load resistance, and  $\varepsilon$  is the dielectric constant.

According to the method from the ISO Guide of the Expression of Uncertainty in Measurement (GUM), the calculation formula of  $A_{eq}$  is as shown in Eq. (1). The relative uncertainty propagation formula of  $A_{eq}$  is deduced as follows,

$$u_r(A_{eq}) = \sqrt{u_r^2(V_{I,p}) + u_r^2(E_p) + u_{rA}^2} \quad (2)$$

where  $u_r(E_p)$  is the relative uncertainty of the standard electric field, and the uncertainty of the field can also be determined by the method introduced from References [11, 12].  $u_{rA}$  is the type A uncertainty for the measurement of repetition.  $u_r(V_{I,p})$  is the relative uncertainty of the integral pulse signal, and the calculation of this uncertainty is the main focus of this paper.

In general, the uncertainty of the digital signal sampled by oscilloscope can be obtained by the parameters of the calibrated oscilloscope. However, the parameters of oscilloscope obtained are not sufficient to attain the uncertainty of the integral value. Therefore, in this paper, the model of the noise in the software integral D-dot measurement system has been built first. Secondly, the uncertainty of integral signal is evaluated at each time point. Additionally, the uncertainty of the peak-peak value of the bipolar pulse is also confirmed. Finally, the uncertainty of the equivalent area of the D-dot sensor is obtained, and some methods for the reduction of the uncertainty of the calibration are provided.

### 3. UNCERTAINTY EVALUATION OF THE INTEGRAL BIPOLAR PULSE SIGNAL

#### 3.1. Background and Idealization for Modeling

The main noise in the D-dot measurement system is the noise from the oscilloscope. The noise mainly consists of two categories [13–16]. The first category includes the quantized noise and other noises in amplitude, and these noises can be treated as stationary additive noises. The second category is the sampling time-base jitter noise. The noise can be treated as non-stationary additive noise, and the standard deviation of second category noise is propagation to the gradient of the signal to be measured [13]. According to the user manual and the calibration report of the Lecory8620A oscilloscope used in the measurement system, the noise caused by the time-base is small and negligible. Thus, the additive noises in the oscilloscope and in other parts of the measurement system are considered concurrently. The sum of the above two noises is defined as the background noise of the D-dot measurement system in this paper.

In order to get an accurate noise value in the measurement system, a more accurate reference signal is required. In the calibration system shown in Figure 2, the uncertainty of the reference electric field is about 2.4%, and the uncertainty of the output of the sensor is about 1.8%. They are similar, and therefore the noise resulting from the subtraction is unsuitable. In this paper, the background noise sampling without signal is analyzed, and the assumption is that this background noise can represent the noise in the D-dot measurement system.

Actually, in order to get the uncertainty of the equivalent area, what is necessary to ascertain is only the integral value in the background noise. Withal, in order to confirm why the model has such a form and why it exhibits the characteristics of the integral value of the noise, we have to formulate a model of the background noise and then make a mathematical derivation. Finally, we have to compare the theoretical model to the test data, to prove the viability of the model.

#### 3.2. Time Domain and Frequency Domain Analysis for the Background Noise

The background noise is sampled when there is no pulse electric field, but other conditions remain the same. The frequency bandwidth of the oscilloscope is 6 GHz, and the sampling rate is 20 GS/s.

In the time domain, the mean value of the data is factored in. The mean value distribution is calculated for different series with the same length (25 ns), and the tendency of mean value with different lengths is also calculated. The typical distribution is shown in Figure 3. The unit of  $y$ -axis is the amplitude of noise divided by voltage per grid in this figure.

After eliminating the mean value (bias), the self-correlation function and spectrum of the background noise are calculated (Figure 4). Self-correlation function is maximum at zero and drastically

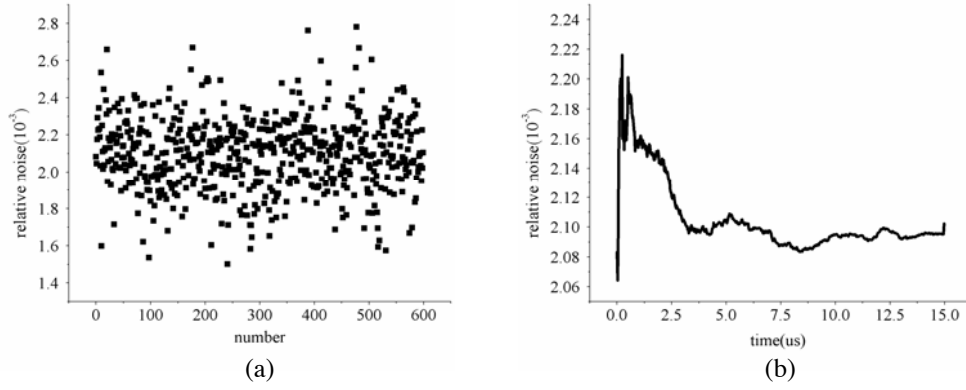


**Figure 3.** The mean value characteristics in the time domain, (a) mean value distribution for different noise series with the same length, (b) tendency of mean value with different lengths.

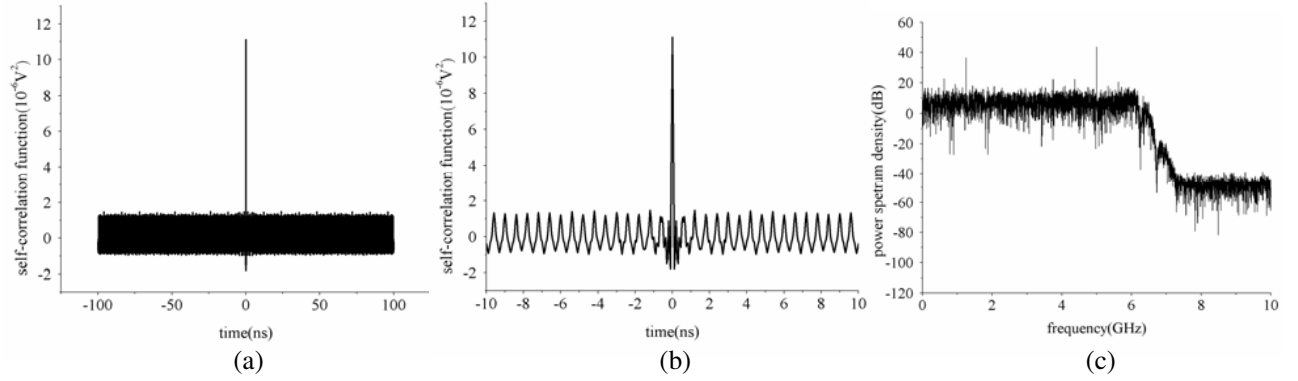


**Figure 4.** Self-correlation function and power spectrum density of the background noise, (a) self-correlation function, (b) partial enlargement self-correlation function, (c) power spectrum density.

decreases as time increases. The limited band of spectrum is 6 GHz, and it is the same as that of the oscilloscope. The characteristics of noise are similar to the white noise.

Then stationarity and normality of the noise are analyzed. The stationarity is evaluated by the athwart order method. The 10 groups of data are divided into 45 segments in each group, and the  $\lambda$  of each group is determined. The background noise has a stationary series of 95% confidence level under the condition that  $|\lambda| < 2$ . The normality is evaluated by the calculation of skewness coefficient  $u$  and kurtosis coefficient  $v$  with the 10 groups of data. The background noise is normal under the condition that  $\hat{u} \approx 0$ ,  $\hat{v} \approx 3$ .

Therefore, the primary conclusion is that the background noise is nonzero mean, stationary, Gaussian random series.

### 3.3. Mathematical Model for the Background Noise

According to the conclusion in Section 3.2, a math model is built for the background noise as follows;

$$W(n) = B + N(n) \quad (3)$$

where  $W(n)$  is the noise series, and  $N(n)$  is the zero mean Gaussian random series with a variance of  $\sigma_N^2$ . In the series, the covariance between variables at different time points is only related to the time interval, so the covariance is represented by  $Cov(j)$ .

The constant bias in the background noise will accumulate to a high level, and the real signal will be concealed by the linear integrated value of the constant bias. A universal method employed for removal

of the bias is that the mean value of the series with the length  $K$  before the pulse signal's arrival is calculated as the estimate of the bias. Thus, the noise after the bias removal is shown as Eq. (4).

$$\bar{W}(n) = W(n) - \sum_{n=1}^K W(n) / K = R + N(n) \tag{4}$$

where  $R$  is the residual error of the bias, and it has an expectation of zero and a variance of  $\sigma_N^2/K + \sum_{i=1}^K 2(K-i)Cov(i)/K^2$ .

The integral error after bias removing is  $I(n)$  as follows,

$$I(n) = Ts \sum_{k=1}^n \bar{W}(k) = Ts \left( nR + \sum_{k=1}^n N(k) \right) = I_R(n) + I_N(n) \tag{5}$$

where  $Ts$  is the sampling interval.  $I_R(n)$  is the integral error of the residual error of the bias. If the bias removal is completed in one operation, it is then a constant. If the bias removal could be operated several times, the error is a random variable with an expectation of zero and a variance of  $\sigma_{I_R}^2(n) = (\sigma_N^2/K + \sum_{i=1}^K 2(K-i)Cov(i)/K^2)(nTs)^2$ .  $I_N(n)$  is the integral error of the zero-mean Gaussian random series. It has an expectation of zero and a variance of  $\sigma_{I_N}^2(n) = Ts^2(n(\sigma_N^2 + \sum_{i=1}^n 2Cov(i)) - 2 \sum_{i=1}^n iCov(i))$ . The covariance between  $I_R(n)$  and  $I_N(n)$  is  $Cov(I_R, I_N) = Ts^2 \frac{n}{K} \sum_{i=1}^K \sum_{j=i+K}^{K+n} Cov(i, j) = Ts^2 \frac{n}{K} \sum_{i=K}^{K+n} Cov(i)$ .

Therefore, for a random measurement, after the random bias removal, the expected value of the integral error is zero, and the variance of the integral value is as follows,

$$\begin{aligned} \sigma_I^2(n) &= \sigma_{I_R}^2(n) + \sigma_{I_N}^2(n) + 2Cov(I_R, I_N) \\ &= Ts^2 \left( n^2 \left( \frac{\sigma_N^2}{K} + \frac{\sum_{i=1}^K 2(K-i)Cov(i)}{K^2} \right) + n \left( \sigma_N^2 + \sum_{i=1}^n 2Cov(i) + \frac{2}{K} \sum_{i=K}^{K+n} cov(i) \right) - 2 \sum_{i=1}^n iCov(i) \right) \end{aligned} \tag{6}$$

### 3.4. Model Verification of the Tested Background Noise Data

A series of background noise data is sampled (the time length is 500  $\mu$ s, and the sampling interval is 50 ps). Then, the noise is divided into several sub-series with specific lengths. The maximum value, expectation value, and variance of the integral value of the noise series at different lengths are estimated by statistics, and the variance of the integral value is compared to the theoretical value in Eq. (10). The variable  $\sigma_N^2$  in Eq. (10) is estimated by the variance of the tested background noise data, and the covariance  $Cov(I_R, I_N)$  is estimated by the self-correlation function. The process of calculation is shown in Figure 5.

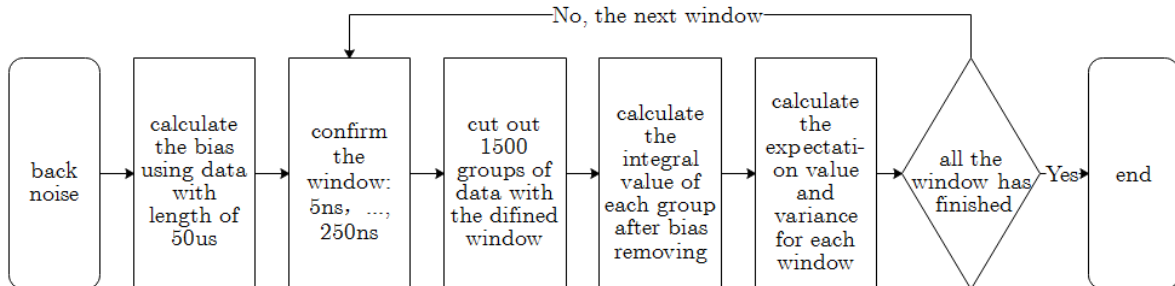
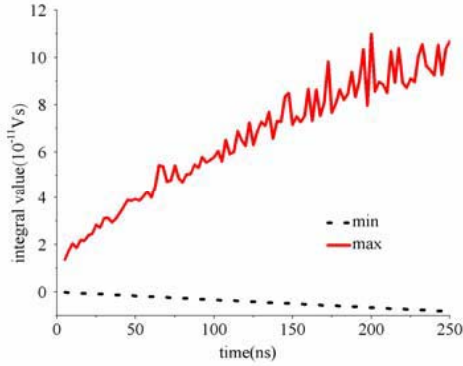
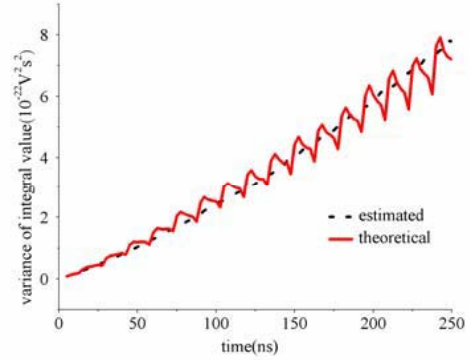


Figure 5. Process used in analyzing the measured background noise.



**Figure 6.** Maximum value and estimated expected value.



**Figure 7.** Comparison between the theoretical variance and estimated variance.

The estimated maximum value and expected value of the integral value of the tested background noise data are shown in Figure 6. The result shows that the estimated expected value of integral value increases with the integral time. It is due to the bias estimated by only one calculation and the existence of a small difference between the estimated bias and real bias. However, when the integral time is far less than the time to calculate the bias, the integral value of the background noise becomes a random variable, and the expected value of the noise is far less than the variance of the noise.

The comparison between the theoretical variance and estimated variance of the integral value of the background noise with the change of integral time is shown in Figure 7. Here, the theoretical value and estimated value have a similar tendency and are almost identical when the integral time is short. Besides, the zigzag jitter is superimposed on the tendency of the theoretical waveform, and the jitter increases with the increase in the integral time. Nevertheless, the jitter in the estimated waveform is small. The possible reason is that the estimated covariance  $Cov(j)$  is not accurate, because of the similar jitter in the self-correlation function (Figure 4).

According to the theoretical modeling and data verification, a reliable model for the integral value of the background noise is set up.

### 3.5. Uncertainty of the Recovery Signal at Every Time Point

According to the model, the uncertainty of the integral signal can be expressed by the standard deviation of the integral value of the background noise. After the integral, the standard deviation can be achieved by two methods. One of the methods is applied when the pure background noise has a short length. In this method, the variance and self-correlation of the background noise are calculated first, and then the standard deviation of the integral value is calculated by Eq. (6). The other method is applied when the pure background noise has a long length. In this method, the standard deviations of the integral value of the background noise series at different lengths are calculated directly by the statistical method.

## 4. AN EXAMPLE FOR THE UNCERTAINTY EVALUATION OF THE EQUIVALENT AREA

According to the model in Eq. (6), for a single measurement, the integral value after the bias removal at every time point can be treated as a Gaussian random variable. The expected value of the integral value is zero, and the variance of the integral value is approximately a quadratic function of the integral time and a linear function of the square of the sampling interval. Therefore, if the variance of the background noise is not affected by the higher sampling rate, the accuracy of the integral signal can be improved by increasing the sampling rate and decreasing the integral time. These data suggest that a suitable oscilloscope and sampling time should be chosen, and the bias removal method should be adopted to reduce the uncertainty of calibration.

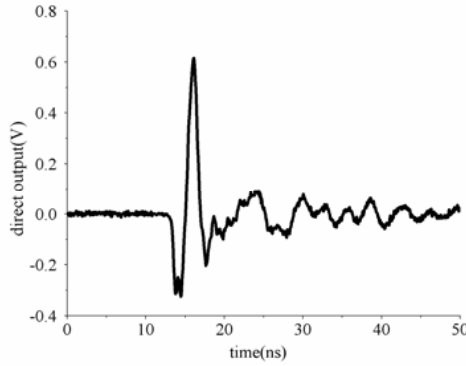


**Figure 8.** The direct output of the D-dot system.

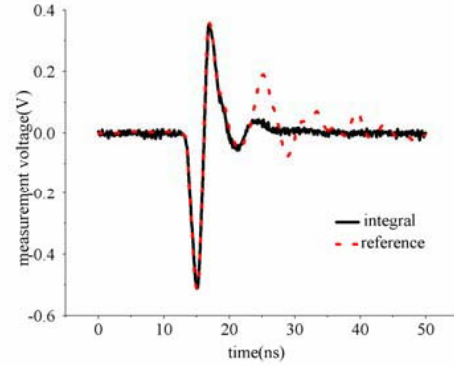


**Figure 9.** Comparison between the reference signal and recovery signal.

Then the calibration data are achieved in the calibration system. The direct output of the D-dot system is shown in Figure 8, and the comparison between the reference signal and recovery signal is shown in Figure 9. In Figure 9, the integral signal has been aligned and amplified to the reference signal.

In Eq. (2),  $u_r(V_{I,p})$  is calculated by the methods shown in Section 3. The vertical grids of the two channels of the oscilloscope are set to 100 mV/div. The peak-peak value of the integral signal is 0.68 nVs (the unit is V\*ns), and the integral time between the positive peak and negative peak is 1.85 ns. The background noises of the two channels used are sampled, and then the difference between the noises of the two channels is integrated with the integral time 1.85 ns several times. The estimated integral error of 1.85 ns is 1.69 pVs. Thus, the relative uncertainty of the peak-peak value is

$$u_r(V_{I,p}) = \frac{1.69 \times 10^{-12}}{0.68 \times 10^{-9}} \approx 0.3\% \quad (7)$$

The uncertainty of the pulse electric field  $u_r(E)$  is 2.4%, and the uncertainty is achieved by a method from [11, 12]. The uncertainty of the peak-peak value in reference signal  $u_r(E_p)$  is  $\sqrt{2.4^2 + 2.4^2} \approx 3.4\%$ . The uncertainty of the repetition measurement for 10 times  $u_{rA}$  is 0.6%. Finally, the uncertainty of the equivalent area of the D-dot sensor is

$$u_r(A_{eq}) = \sqrt{3.4^2 + 0.6^2 + 0.3^2} \approx 3.5\% \quad (8)$$

## 5. CONCLUSIONS

In this paper, a method to evaluate the uncertainty of the equivalent area of the D-dot sensor in a software integral system is formulated. In this method, the sensors are calibrated in the standard field generation equipment. A mathematical model of the integral error of background noise in the D-dot system is formulated. According to the model, the calibration uncertainty evaluation problem is solved. The model shows how background noise in the software integral D-dot system influences the accuracy of calibration and measurement. Importantly, it provides us with some methods of reducing the uncertainty of the calibration. The model can not only be used to evaluate the uncertainty of the D-dot sensor in a software integral system but also be meaningful in solving similar problems in other software integral systems.

## REFERENCES

1. Liu, X., Y. Fan, G. Liu, et al., "Investigation of ultra-wide band transient electromagnetic field measurement," *High Power Laser and Particle Beams*, Vol. 11, No. 06, 742–746, 1999.
2. Zhu, S., B. Zhu, and Y. Fan, "Measurement system of ultra-wide spectrum electromagnetic pulse radiating field," *High Power Laser and Particle Beams*, Vol. 18, No. 2, 261–264, 2006.

3. Jing, X., X. Zheng, and Y. Sun, "Research on the technology of EMP measurement in time-domain," *Journal of Microwaves*, No. S2, 76–78, 2010.
4. Alferness, R. C., "Waveguide electropititc mosulators," *IEEE Transactions on Microwave Theory and Techniques*, Vol. 30, No. 8, 1121–1137, 1982.
5. Ferrero, A., "Measuring electric power quality problems and perspectives," *Measurement*, Vol. 41, 121–129, 2008.
6. He, W., R. Luo, J. Wang, et al., "Principles and experiments of voltage transformer based on self-integrating D-dot probe," *Proceedings of the CSEE*, Vol. 34, No. 15, 2445–2451, 2014.
7. Chen, J., X. Cui, X. Liu, et al., "Ultra-wideband standard antenna for transient field measurement of short electromagnetic pulse," *Proceedings of the 2013 International Symposium on Electromagnetic Compatibility*, 197–202, 2013.
8. Olsen, S. L., "Asymptotic conical dipole D-dot sensor development," AFWL-TR-75-263, 1976.
9. Wang, Q., Y. Li, and L. Shi, "Design and experimental research of D-dot probe for nuclear electromagnetic pulse measurement," *High Power Laser and Particle Beams*, Vol. 27, No. 11, 233–239, 2015.
10. Yao, L. J., et al., "Compensation of the offset in numerical integration of a D-dot sensor measurement," *Proc. 3rd Asia-Pac Conf Antennas Propag.*, 898–901, 2014.
11. Yan, Y., T. Jiang, X. Liu, et al., "Traceability and uncertainty of ultra-wide band short pulse electric field standard device," *High Power Laser and Particle Beams*, Vol. 26, No. 6, 2014.
12. Yan, Y., T. Jiang, J. Chen, et al., "Study of the time-domain electromagnetic pulse standard field generation setup and its application," *Review of Scientific Instruments*, Vol. 89, 074703, 2018.
13. Tamas, D., "Uncertainty of signal reconstruction in the case of jittery and noisy measurement," *IEEE Transactions on Instrumentation and Measurement*, Vol. 47, 1062–1065, 1998.
14. Liang, Z. and X. Meng, "Study on evaluation of both time-base distortion and sampling jitter of digital storage oscilloscopes," *Acta Metrological Sinica*, Vol. 29, No. 4, 358–364, 2008.
15. Liang, Z. and X. Meng, "Review of sampling jitter research," *Journal of Test and Measurement Technology*, Vol. 23, No. 3, 253–260, 2009.
16. Zhu, J., R. Li, J. Miao, et al., "Time-based distortion correction algorithm of high-speed sampling oscilloscope," *Journal of Beijing University of Technology*, Vol. 39, No. 12, 1810–1814, 2013.
17. IEEE Std 1309TM-2013, "IEEE standard for calibration of electromagnetic field sensors and probes(excluding antennas) from 9 kHz to 40 GHz," *IEEE Electromagnetic Compatibility Society*, 2013.